MODEL SIMULATION OF CONVECTIVELY LOFTED ICE CONTRIBUTION TO STRATOSPHERIC WATER VAPOR

A Thesis

by

WANDI YU

Submitted to the Office of Graduate and Professional Studies of
Texas A&M University
in partial fulfillment of the requirements for the degree of

MASTER OF SCIENCE

Chair of Committee,	Andrew Dessler
Committee Members,	Kenneth Bowman
	Ping Yang
	Robert Hetland
Head of Department,	Ping Yang

December 2017

Major Subject: Atmospheric Sciences

ABSTRACT

Changes in the amount of stratospheric water vapor can affect both the chemistry and climate in the stratosphere and troposphere. Convectively lofted ice near and above the tropopause can evaporate and contribute to stratospheric water vapor. Here we conduct several experiments using a trajectory model driven by two chemistry-climate models (CCMs) to study the contribution of lofted ice to stratospheric water vapor. We show that the largest amount of evaporation of convectively lofted ice occurs in the Tropical Tropopause Layer (TTL) and above the Lagrangian cold point, and we find two key regions for lofted ice evaporation: the Asian monsoon region during JJA (June, July, and August) and the tropical western Pacific during DJF (December, January, and February), regions where convection frequently occurs and the evaporation rate of lofted ice is high. The distribution of net contribution is mainly determined by the degree of subsaturation in the TTL, and the net contribution of lofted ice is then transported to the rest of the stratosphere by the general circulation. Over the 21st century, an increase of subsaturation leads both the lofted ice evaporation rate and the net contribution to increase. It explains part of the increase of stratospheric water vapor over the 21st century.

ACKNOWLEDGMENTS

It has been three years since I begin my graduate research in department of atmospheric sciences in Texas A&M University. This is my first research program, and to begin is always the hardest thing. Without the help of a lot of people, I wound not have the works done.

I would like to first thank my advisor, Dr Andrew Dessler. He not only gave me a lot of advise on my research, but also guide me to get familiar with how to do research, how to get ideas, and how to deal with the difficulties one may face while doing research.

I would like to acknowledge the professors in my committee, especially Dr Kenneth Bowman, for their guidance and help. I would also like to thank people in our research group, Brooke Adams, Hao Ye, Jeffrey Mast, and Xun Wang. Also thank people in our department, Kevin Smally, Jiachen Ding, and Steve Schroeder, for giving me advises on my thesis and defense.

Finally, I must express my gratitude to my parents. They gave me a lot of support when I decide to go abroad and continue my study. They are always the most important people to me in the world.

CONTRIBUTORS AND FUNDING SOURCES

Contributors

This work was supported by a thesis committee consisting of Professors Andrew Dessler, Kenneth Bowman, and Ping Yang of the Department of Atmospheric Science and Professor Robert Hetland of the Department of Oceanography.

All other work conducted for the thesis was completed by the student independently.

Funding Sources

This work is supported by NASA grant NNX14AF15G.

NOMENCLATURE

TTL	Tropical tropopause layer
DJF	December, January, and February
JJA	June, July, and August
CCM	Chemistry climate model
GEOSCCM	Goddard Earth Observing System Chemistry Climate Model
WACCM	Whole Atmosphere Community Climate Model
traj_GEOSCCM	Trajectory model result driven by GEOSCCM
traj_WACCM	Trajectory model result driven by WACCM
RCP	representative concentration pathways
ppmv	part per million by volume
AS	Asian monsoon region
TWP	Tropical western Pacific

TABLE OF CONTENTS

Page

LIST OF FIGURES

FIGURE Page

LIST OF TABLES

TABLE Page

1. INTRODUCTION

1.1 Stratospheric water vapor

1.1.1 Importance of stratospheric water vapor

Stratospheric water vapor is important to stratospheric chemistry; it is a primary source of OH hydroxyl radicals, an important oxidizing agent that participates in the control of ozone [Evans et al., 1998; Stenke and Grewe, 2005]. The chemical and radiative characteristics of stratospheric water vapor also make it an important factor for Earth's climate [Forster and Shine, 2002; Solomon et al., 2010; Dessler et al., 2013]. Studies of the response of stratospheric temperature, water vapor, and ozone showed that an increase of stratospheric water vapor could lead to loss of ozone, and thus cause stratospheric cooling [Ramaswamy et al., 1996; de F. Forster and Shine, 1999; Dvortsov and Solomon, 2001; Smith et al., 2001]. Model simulations also showed that an increase of stratospheric water vapor could have a warming effect on surface temperature [de F. Forster and Shine, 1999; Shindell, 2001]. Furthermore, the long-term trend of stratospheric water vapor can then impact stratospheric temperature and wind, and also impact atmospheric circulation [Maycock et al., 2013].

1.1.2 Sources of stratospheric water vapor

The transition between the troposphere and stratosphere over the tropics is referred to as the tropical tropopause layer (TTL) [Sherwood and Dessler, 2000; Fueglistaler et al., 2009], which is located between 355 K and 425 K potential temperature, corresponding to pressures between 150 hPa and 70 hPa, and altitudes between approximately 14 km and 18.5 km. Significant convective detrainment happens in this layer [Dessler, 2002], which strong effects its composition and structure.

Brewer [1949] suggested that most air enters the stratosphere and is dehydrated around the tropical tropopause; it is then transported to mid-and-high-latitudes and Polar Regions. The most important factor determining the stratospheric water vapor budget is dehydration that occurs while passing through the TTL, which is largely controlled by the coldest temperatures found there [Mote et al., 1996; Randel et al., 2004; Fueglistaler and Haynes, 2005]. Large-scale variability, like that from the quasi-biennial oscillation (QBO) and El Nino-Southern Oscillation (ENSO), can affect TTL temperature, thereby influencing the interannual variability of stratospheric water vapor [Geller et al., 2002; Scaife et al., 2003 Bonazzola and Haynes, 2004; Randel et al., 2004; Dessler et al., 2013; Tao et al., 2015].

Another important contributor to stratospheric water vapor is oxidation of methane [Bates and Nicolet, 1950] in the upper stratosphere. The best estimate is that oxidation of each methane generates between 1.5 and 2.0 molecules of water vapor [Jones et al., 1986; Le Texier et al., 1988; Hansen and Robinson, 1989; Gunson et al., 1990; Dessler et al., 1994] and the approximation $dH_2O/dCH_4 = 2$ is widely accepted.

Finally, convective overshooting brings cloud ice into the TTL, where it can evaporate and moisten the stratosphere [Grosvenor et al., 2007; Liu et al., 2010a]. Importantly, this convection bypasses the cold point, disconnecting stratospheric water from TTL temperatures.

1.2 Deep convective clouds

The aim of this thesis is to study and quantify the moistening impact of convectively lofted ice on stratospheric water vapor in two chemistry-climate models (CCMs). Observations have shown that convective clouds are ubiquitous in the TTL. High resolution global satellite imagery of cloud brightness temperatures showed that convection penetrates up to 1.5 km above the tropopause [Gettelman et al., 2002]. Observations from the precipitation radar on the Tropical Rainfall Measuring Mission (TRMM) showed that 5%

of the deep convection could reach beyond the tropopause [Alcala and Dessler, 2002]. A different analysis of TRMM data showed that 1.3% of convection systems could reach 14 km ($\sim$ 355 K potential temperature) and 0.1% could reach 16.5 km ($\sim$ 380 K potential temperature) [Liu and Zipser, 2005]. A study analyzing 22 years of infrared satellite data [Rossow and Pearl, 2007] showed that large convective systems could penetrate into the TTL and lower stratosphere. Furthermore, radar data from the Global Precipitation Mission (GPM) observations also showed that deep convection could reach the tropopause and beyond [Liu and Liu, 2016]. Calculations of mass detraining in the TTL suggest that convection is detraining significant amounts of mass as high as 380 K potential temperature [Dessler, 2002].

It has long been speculated that convective clouds in the TTL play an important role in the stratospheric water vapor budget. Some early work focused on the hypothesis that these clouds dehydrated the stratosphere. Early work done by Danielsen [1982] suggested that radiative cooling at convective anvil top could serve as an explanation of the low stratosphere water vapor mixing ratio. Sherwood and Dessler [2000] also suggested that convective overshoot and mixing of dry convective air could dehydrate the TTL.

More recently, the preponderance of evidence has suggested that these clouds hydrate the TTL and lower stratosphere. Kley et al. [1982] analyzed aircraft data and concluded that convective storms provide water to stratosphere. A field campaign that took place in Bauru, Brazil showed that convective overshooting clouds could hydrate the lower stratosphere and the enhanced H_2O mixing ratio reached as high as 10 ppmv [Nielsen et al., 2007]. Observations by aircraft over San Paulo, Brazil and later simulations showed that deep convective systems could penetrate the stratosphere and moisten the air up to 420 K potential temperature [Chaboureau et al., 2007; Corti et al., 2008]. During the SCOUT-AMMA campaign over Africa, several cases of convective overshoot were detected by soundings, and the water vapor mixing ratio was found to be enriched by 1-3

ppmv [Khaykin et al., 2009; Liu et al., 2010b]. Study of the isotopic composition of stratospheric water vapor implies that convective lofting and evaporation of cloud ice is necessary to explain the distribution of stratospheric HDO, a stable isotopologue of water [Moyer et al., 1996; Keith, 2000; Dessler et al., 2007]. Meanwhile, model simulations combining convection and cloud ice microphysics processes showed that moistening by convectively lofted ice improves comparison with observations [Schoeberl et al., 2014; Ueyama et al., 2015].

1.3 Motivation and previous study

Processes in the TTL primarily control stratospheric water vapor, and there are two processes that we focus on: dehydration caused by low TTL temperatures, and hydration from the evaporation of convectively lofted cloud ice.

Most air entering the stratosphere experiences its final dehydration in the TTL, so the concentration of water vapor entering the stratosphere from the TTL will be referred as H_2O_{entry}. Previous work analyzing the evaporation of lofted ice and its impact on long-term trends in H_2O_{entry} in chemistry-climate model (CCM) simulations was done by Dessler et al. [2016]. They found that lofting of ice into the lower stratosphere moistened the lower stratosphere, playing a key role in the long-term trend over the 21st century.

Although most evidence suggests that the evaporation of convectively lofted ice can moisten the stratosphere, the details of ice evaporation in the TTL have yet to be studied. In this thesis, we will extend Dessler et al. [2016]'s analysis and look in detail at the time and space scales of overshooting convection and convective hydration of the TTL using two CCMs.

2. MODEL AND METHOD

2.1 The trajectory model

In all of the experiments in this thesis, a Lagrangian domain-filling forward trajectory model is used [Schoeberl and Dessler, 2011; Schoeberl et al., 2012; Schoeberl et al., 2013] to simulate the evolution of water vapor in the TTL and stratosphere. This is a Lagrangian model: the trajectory of individual parcels, instead of flow at fixed positions, is calculated using simulated from global chemistry climate models. The experiments uses a domain filling strategy: parcels are initialized every day in the TTL, above the level of zero radiative heating in the tropics, so parcels tend to ascend through the cold point tropopause (minimum temperature) where they are dehydrated. The location where a parcel go through the coldest temperature along its trajectory is designated the Lagrangian cold point for that parcel. As the model runs, the stratosphere fills with parcels, allowing us to investigate the three-dimensional structure of tracer fields and the associated mass transport.

Trajectories are computed using the TRAJ3D trajectory model [Bowman, 1993; Bowman and Carrie, 2002]. Vertical velocities in isentropic coordinates are computed from 6-hourly average diabatic heating rates. Horizontal velocities come from 6-hourly instantaneous two-dimensional horizontal wind fields.

We drive the trajectory model with meteorological fields from two chemistry-climate models (CCMs). One is the Goddard Earth Observing System Chemistry Climate Model (GEOSCCM), which couples the GEOS-5 general circulation model [Rienecker et al., 2008; Molod et al., 2012], with a comprehensive stratospheric chemistry model. This model has 72 vertical levels, with horizontal resolution 2°latitude by 2.5°longitude. In this thesis, we use a simulation driven by the Representative Concentration Pathway (RCP) 6.0

scenario for greenhouse gases [Van Vuuren et al., 2011], and the A1 scenario for ozone depleting substances [World Meteorological Organization, 2011] from 1998 to 2099. The trajectory experiments driven by GEOSCCM output will be referred as traj_GEOSCCM runs.

We also drive the trajectory model with meteorological fields from the Whole Atmosphere Community Climate Model (WACCM), a version of the Community Earth System Model (CESM) [Hurrell et al., 2013; Marsh et al., 2013]. We use a specified chemistry version of WACCM (SC-WACCM), which is a simplified version where ozone and other constituents, as well as short wave radiation, are prescribed from earlier WACCM simulations [Smith et al., 2014]. The resolution of SC-WACCM is 1.9°latitude by 2.5°longitude on 66 vertical levels. In this thesis, we use a simulation driven by the RCP 8.5 greenhouse gas scenario [Van Vuuren et al., 2011], from 1955 to 2100. The experiments driven by WACCM output will be referred as traj_WACCM runs.

The experimental design is similar to that used by Dessler et al. [2016]: each day 1350 parcels are released at 370 K ($\sim$16 km) on an equal area grid between 60°N and 60°S. Parcels are removed if they descend to altitudes below 250 hPa ($\sim$10 km), or if they ascend to altitudes above either 0.001 hPa or 5000 K. The time step of the trajectory model is 45 minutes.

Each parcel is initialized with a water vapor mixing ratio of 200 parts per million by volume (ppmv). The water vapor mixing ratio is conserved along the trajectory path unless the parcel exceeds a relative humidity (RH) threshold; when that happens, water vapor is instantly removed to limit the parcel to that threshold RH. We set the RH threshold to be consistent with the corresponding CCM's RH threshold. In the GEOSCCM [Molod, 2012], condensation occurs below 100% RH, so in traj_GEOSCCM experiments, we set the RH threshold to be 80% (referred to as s80 runs). In WACCM, condensation occurs 100% RH [Neale et al., 2010; Marsh et al., 2013], so we set the RH threshold in

traj_WACCM experiments to 100% (referred to as s100 runs).

The loss rate of methane comes from the photochemical loss rates in the Goddard two-dimensional model [Fleming et al., 2007; Schoeberl and Dessler, 2011]. Water vapor from methane oxidation is added to parcels every 6 hours; here we use the widely accepted approximation that each molecule of methane oxidized adds two molecules of H_2O [Gunson et al., 1990; Dessler et al., 1994].

When a parcel goes through a convective cloud region, lofted ice will be added. We use 6-hourly three-dimensional anvil ice data from GEOSCCM – which is ice only from convective events – and 6-hourly three-dimensional cloud ice data from WACCM – which includes both convective and in situ clouds – in our trajectory simulations. Using linear interpolation in both time and space, the cloud ice field is interpolated to the parcel's trajectory each time step. The evaporation of lofted ice is complete, and the evaporated lofted ice is immediately added to the parcel water vapor content, until the parcel encounters the relative RH threshold. For comparison, we also perform several experiments with the same settings, except that we do not add lofted ice in these experiments (referred to as no-ice runs while the experiments of adding lofted ice is referred to as ice runs).

To quantify the contribution of lofted ice, we calculate the lofted ice evaporation rate as the average difference between H_2O before and after the ice evaporation step of the trajectory model. Multiplying this by the number of steps per day, 32, yields the average ice evaporation rate per day. We will also calculate the net contribution of lofted ice by subtracting water vapor mixing ratio in the ice runs from the corresponding no-ice runs. The ice evaporation rate is an instantaneous variable showing the source of evaporated lofted ice, while the net contribution illustrates the total contribution from lofted ice to stratospheric water vapor. These quantities differ because some of the ice evaporate included in the former statistic can be subsequently dehydrated out and won't affect the latter.

We compare two time periods in our experiments: January 1 2000 through December

31 2009, and January 1 2089 through December 31 2098. We drop the first year of each model run to ensure that spin-up issues don't affect our results.

2.2 Temperatures and lofted ice fields in the CCMs

The horizontal distribution of temperatures in the CCMs during 2000-2009 and the difference between them at 85 hPa, a level near the top of the TTL, is shown in fig. 2.1. In both CCM runs, the coldest temperatures are found over the tropical western Pacific and South America during DJF (December, January and February) and the tropical cold centers are over the Asian monsoon region and the western Pacific during JJA (June, July, and August).

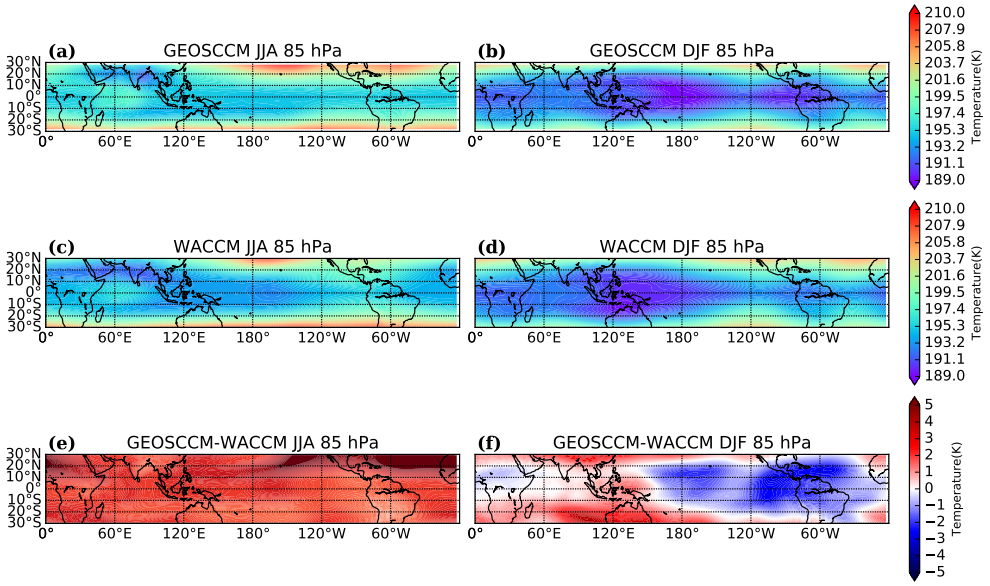

Figure 2.1: Tropical temperature field at 85 hPa over 2000-2009 in (a-b) GEOSCCM, and in (c-d) WACCM; (e-f) The difference between GEOSCCM and WACCM temperature field. Left panels show JJA and right panels show DJF.

The horizontal distribution of DJF anvil ice mixing ratio in GEOSCCM output in the TTL is shown in fig. 2.2a, c and e. Anvil ice is mainly located within the tropics (30°N to 30°S), and has similar pattern on different levels. Centers of anvil ice are found above the tropical western Pacific, South America, and South Africa.

The vertical distribution in fig. 2.2g shows that the amount of anvil ice decreases with height, with almost no ice over 70 hPa. The distribution pattern of cloud ice in WACCM, shown in fig. 2.2b, d, f, and h is similar to that in GEOSCCM, while the amount of cloud ice is much higher, as a result of containing both lofted ice and ice formed in situ.

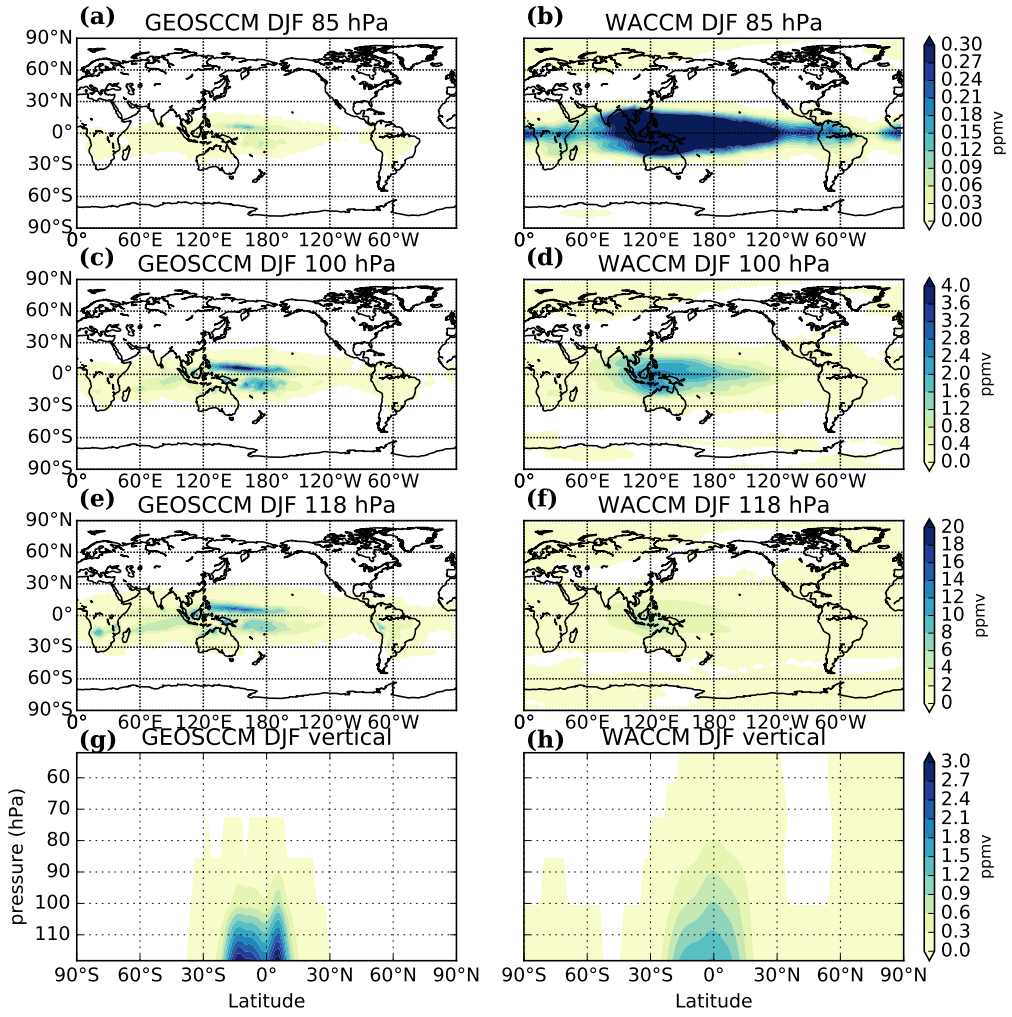

Figure 2.2: (Left panels) GEOSCCM anvil ice mixing ratio, and (right panels) WACCM cloud ice mixing ratio during DJF over 2000-2009, at (a,b) 85 hPa, (c,d) 100 hPa, (e,f) 118 hPa, and (g,h) global average vertical distribution by latitude and pressure.

Cloud ice in JJA is shown in fig. 2.3. Anvil ice during JJA in GEOSCCM output is also found throughout the tropics, and mainly located over India, and the Indian Ocean (regions around the Asian monsoon), and extending into the tropical western Pacific. Cloud ice in WACCM output during JJA is mainly over the Asian monsoon region. The vertical distribution of ice in GEOSCCM and WACCM, shown in fig. 2.3g and h, also decreases

with height, and the majority of cloud ice is located within the tropical area and below 60 hPa. In general, the average cloud ice mixing ratio and cloud top altitude during JJA is lower than during DJF.

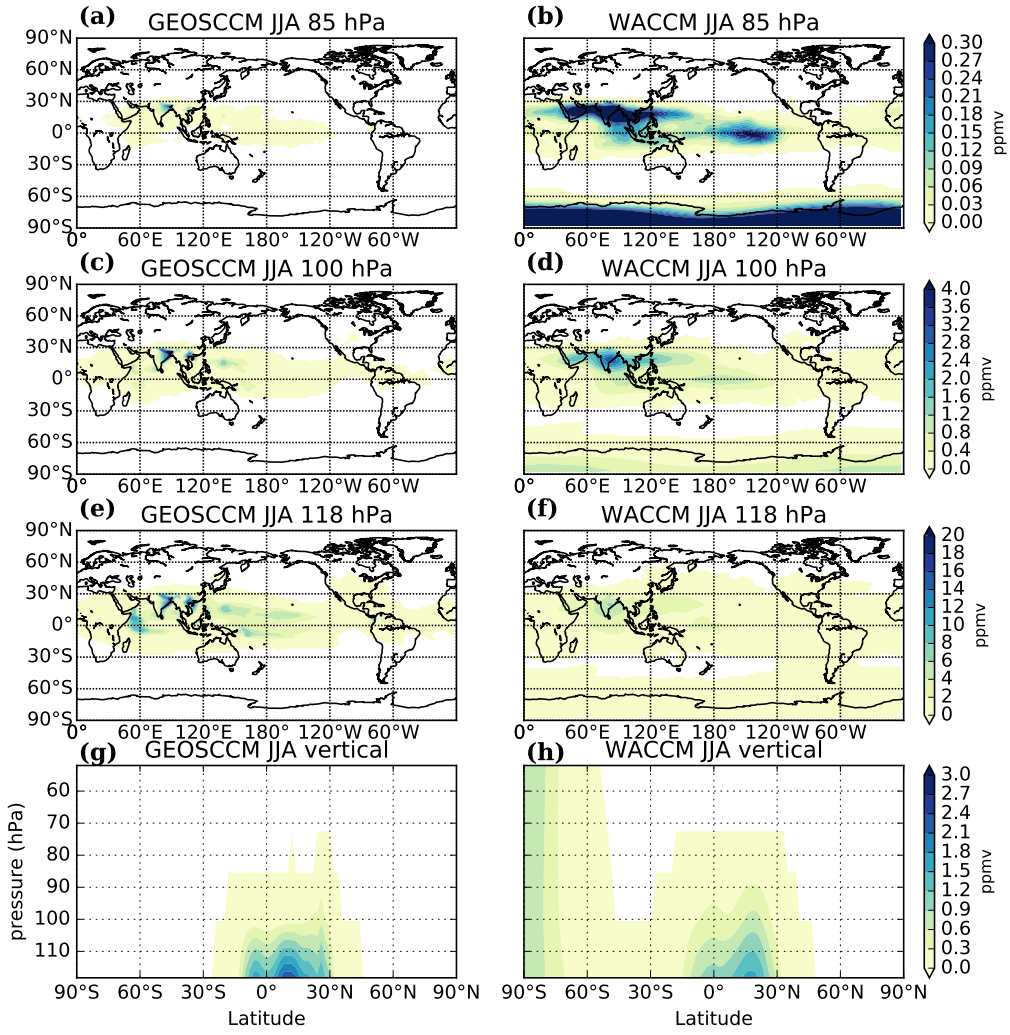

Figure 2.3: (Left panels) GEOSCCM anvil ice mixing ratio, and (right panels) WACCM cloud ice mixing ratio during JJA over 2000-2009, at (a,b) 85 hPa, (c,d) 100 hPa, (e,f) 118 hPa, and (g,h) global average vertical distribution by latitude and pressure.

During both JJA and DJF, there are clouds in the polar regions in WACCM. These are

clouds formed in situ due to very cold temperatures found there and may act to dehydrate the polar regions if they sediment out. This process is not relevant to what we are studying and does not influence our results.

The cloud ice data from both CCMs agrees well with satellite and radar observations. Gettelman et al. [2002] showed that the amount of clouds from convective overshoots is higher during DJF, especially over the central and western Pacific in February and over the Asian Monsoon in August. Similar conclusions have been drawn by Rossow and Pearl [2007], suggesting that convective penetrating clouds are concentrated over the eastern Indian Ocean and western Pacific Oceans, over the western end of South Pacific Convergence Zone, the eastern end of the Pacific Intertropical Convergence Zone, and over South America and South Africa. Liu and Zipser [2005] suggested that most convective overshooting events occur over land, especially over central Africa, Indonesia, and South America.

2.3 Assumption of convective cloud top in traj_WACCM

Analysis of the traj_WACCM is more complicated than for traj_GEOSCCM because its cloud ice fields include both convectively lofted ice as well as ice formed in situ in the TTL. Clouds formed in situ condense local TTL water, so their subsequent evaporation is not a net source of water. So allowing all of the cloud ice in the traj_WACCM to evaporate may add too much water to the TTL. To account for this, we define a convective cloud top and assume cloud ice below this level is convectively lofted cloud ice that evaporates and hydrates the TTL, while ice above this level is formed in situ and whose evaporation does not hydrate the TTL.

To determine the altitude of convective cloud top, several traj_WACCM experiments have been done. In each one, we constrain ice evaporation below a particular pressure level. Fig. 2.4a shows tropical average water vapor mixing ratio from WACCM and from

various trajectory runs over the 2000-2009 period, indicating that allowing ice below 90 hPa to evaporate provides the closest match to the WACCM profile. Thus, in the following experiments driven by WACCM output we only allow cloud ice to evaporate at altitudes below 90 hPa. This threshold applies to runs over the period 2000-2009.

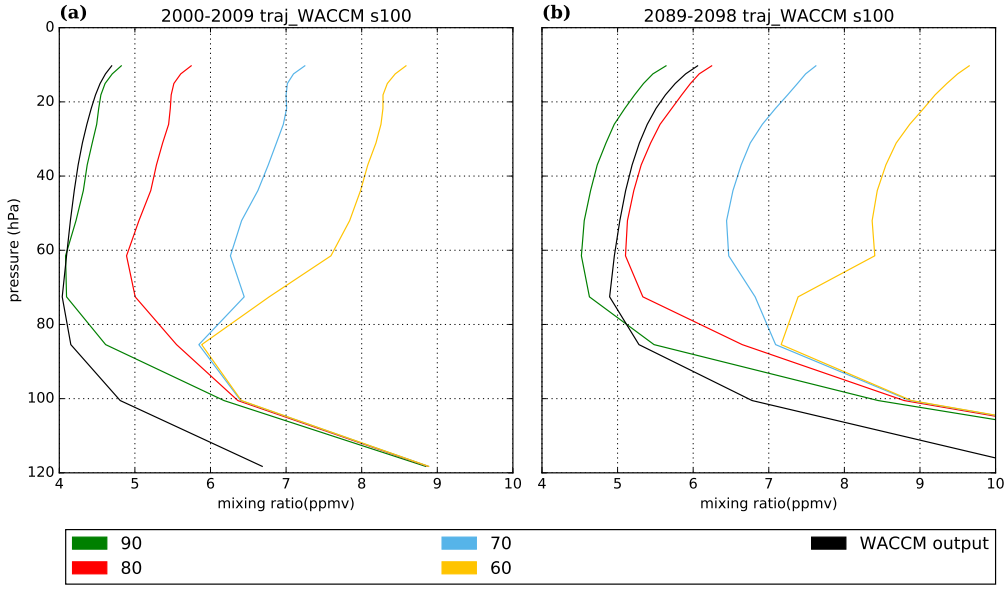

Figure 2.4: Tropical average H_2O mixing ratio in several traj_WACCM s100 run, and tropical average H_2O mixing ratio in WACCM output over 2000-2009 (a), and over 2089-2098 (b). In these experiments, cloud ice is allowed to evaporate below a set level: 90 hPa, 80 hPa, 70 hPa, and 60 hPa.

Our thesis also concerns the changes of evaporation rate and net contribution of lofted ice over the 21st century. Almost all models predict that, over the 21st century, the troposphere gets warmer and the stratosphere gets colder, accompanied by a warmer and high cold point tropopause [Santer et al., 2003; Gettelman et al., 2010]. Because of this, the cutoff altitude where we assume ice changes from convective to in situ should increase over the 21st century, and we need to define a second convective cloud top for the end of

the century. Fig. 2.4b shows that over 2089-2098, the closest match to the WACCM is the experiment that allows lofted ice to evaporate below 80 hPa, so this is the convective cloud top we assume in the traj_WACCM runs covering the 2089-2098 period.

2.4 Convective contrast in trajectory no-ice experiments

The evaporation of convectively lofted ice needs a subsaturated environment, while the degree of subsaturation is connected to the TTL temperatures. This means that the amount of subsaturation is a bridge that connects temperature and the evaporation of lofted ice, and we need to know more precisely how much evaporated ice can be added. To better quantify the degree of subsaturation, we define the convective contrast before adding evaporated lofted ice as:

$$Convective\ contrast = MR^{s}_{H_2O} * RH_{thresh} - MR_{H_2O} \tag{2.1}$$

Here $MR^{s}_{H_2O}$ is the saturated H_2O mixing ratio and MR_{H_2O} is the H_2O mixing ratio in the no-ice trajectory experiments; RH_{thresh} is the RH threshold we use, 80% in traj_GEOSCCM and 100% in traj_WACCM. Dessler and Sherwood [2004] presented this concept, suggesting that the contrast between the abundance of H_2O and the local saturation H_2O mixing ratio is important in determining the amount of convective moistening in mid-latitude summer. We will test this conclusion in the trajectory model to evaluate whether it helps us understand the model's behavior. The convective contrast at 85 hPa is shown in fig. 2.5a-d. Although temperatures in WACCM are much lower than in GEOSCCM, the values of convective contrast in the models are similar. The distribution of convective contrast is consistent with the temperature field in CCMs: cold regions are nearly saturated and have low convective contrast, and warm regions are dry and have high convective contrast. The correspondence between temperature and convective contrast is not linear but exponential, so a warm area can have an extremely large convective contrast.

The areas we are interested in are the convective cloud centers in each season: the Asian monsoon region (10°N-30°N, 50°E -100°E) during JJA, and the tropical western Pacific (10°S-10°N, 100°E -160°W) during DJF. We notice that they are also regions with low convective contrast (fig. 2.5). The convective contrast over the Asian monsoon during JJA is 2.89 (in traj_WACCM)-3.84 (in traj_GEOSCCM) ppmv. This is much higher than the convective contrast over the tropical western Pacific during DJF, which is 1.52 (in traj_WACCM)-1.65 (in traj_GEOSCCM) ppmv. During JJA, the TTL has larger moistening potential from the evaporation of convectively lofted ice than during DJF.

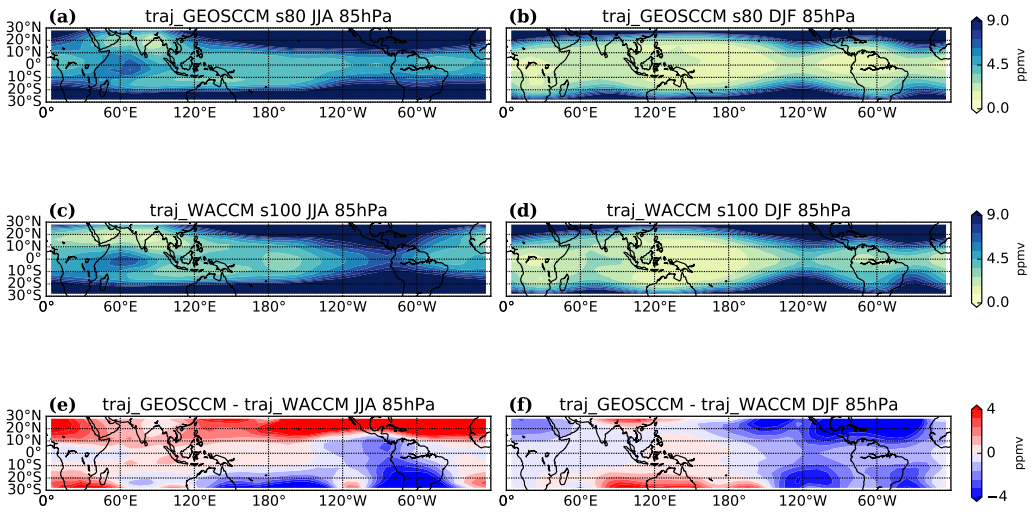

Figure 2.5: Convective contrast at 85 hPa over 2000-2009 in (a, b) traj_GEOSCCM, and in (c, d) traj_WACCM; (e-f) The difference between traj_GEOSCCM and traj_WACCM convective contrast. Left panels show JJA and right panels show DJF.

Comparing the convective contrast between traj_GEOSCCM and traj_WACCM, we find that although the convective contrast in traj_GEOSCCM is lower than that in traj_WACCM over some tropical regions, it is higher over these two key regions (the Asian

monsoon region during JJA, and the tropical western pacific during DJF). This means that the evaporation of lofted ice in traj_GEOSCCM has a greater potential to moisten the stratosphere.

3. LOFTED ICE EVAPORATION AND CONTRIBUTION

We now quantify the impact of lofted ice on lower stratospheric water vapor. To begin, we define H_2O_{entry}, the humidity of air entering the stratosphere, as the tropical (30°N to 30°S) average water vapor mixing ratio at 85 hPa, a level near the top of the TTL, so both dehydration and evaporation of lofted ice above this level will have a relatively small impact on water vapor. Dessler et al. [2016] showed that adding lofted ice into the trajectory model can improve the simulation of both the average of H_2O_{entry} over the 21st century and the change in H_2O_{entry} over 21st century.

In this thesis, our focus is on the monthly variability of water vapor, not the absolute value, so we subtract the average seasonal cycle from monthly mean H_2O_{entry} to get the monthly anomaly, ΔH_2O_{entry}. Fig. 3.1 shows time series of ΔH_2O_{entry} from the trajectory models and from the CCMs, indicating that ΔH_2O_{entry} in the CCMs is well simulated by both the trajectory runs with and without ice and for both traj_GEOSCCM and traj_WACCM experiments. The correlation coefficients between trajectory ΔH_2O_{entry} and CCM ΔH_2O_{entry} are shown in Table 3.1. All the four correlation coefficients pass a significance test at the 0.95 level.

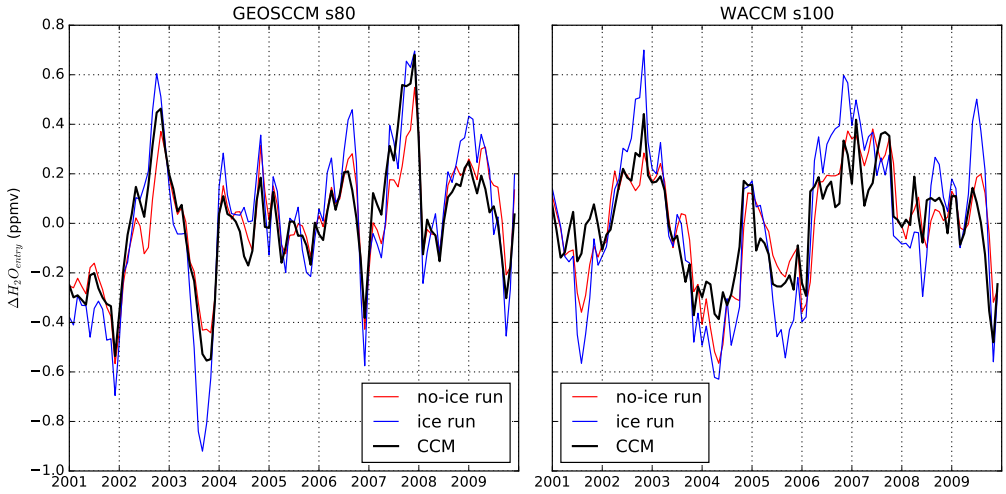

Figure 3.1: ΔH_2O_{entry} from 2001 to 2009 in the trajectory model no-ice runs and ice runs results, and CCMs. Monthly anomaly ΔH_2O_{entry} is calculated by subtracting monthly climatology from monthly mean H_2O_{entry}, and H_2O_{entry} is the tropical average H_2O mixing ratio at 85 hPa. (a) shows traj_GEOSCCM s80 and GEOSCCM, (b) shows traj_WACCM s100 and WACCM. ΔH_2O_{entry} is monthly anomaly of the tropical average water vapor mixing ratio at 85 hPa.

Table 3.1: Correlation coefficients (r) and root mean square errors (rms error) between trajectory model ΔH_2O_{entry} and CCM ΔH_2O_{entry} over 2001-2009. ΔH_2O_{entry} is the monthly anomaly of the tropical average water vapor mixing ratio at 85 hPa.

	traj_GEOSCCM s80		traj_WACCM s100	
	r	rms error	r	rms error
no-ice run	0.918	0.095	0.827	0.122
ice run	0.930	0.136	0.864	0.177

In the no-ice runs, the only factor that determines ΔH_2O_{entry} is temperature. The agreement between the CCMs and the no-ice runs shows that temperature explains most

of the variance of ΔH_2O_{entry}, a result in agreement with previous analyses [Brewer, 1949; Mote et al., 1996; Randel et al., 2004; Fueglistaler and Haynes, 2005; Schoeberl and Dessler, 2011; Dessler et al., 2014]. In the ice runs, evaporation of convectively lofted ice also influences ΔH_2O_{entry}. Ice runs have slightly higher correlation coefficients with CCM than no-ice runs have with CCM. The differences between the no-ice and the ice runs are small, suggesting that evaporation of convectively lofted ice plays a small role on interannual time scales. Dessler et al. [2016] reached this same conclusion, but also showed that on centennial time scales lofted ice plays a much more important role. The RMS errors in the ice runs are higher than in the no-ice runs, as a result of overestimating the peak-to-peak variation. A possible reason for the overestimate is that we do not consider microphysical process and allow the lofted ice to evaporate immediately.

RMS errors in traj_GEOSCCM runs are lower, and the correlation coefficients higher, than in traj_WACCM runs, indicating that the trajectory model does a better job simulating the GEOSCCM field than it does for WACCM.

3.1 Lofted ice evaporation rate

Previous studies showed that the evaporation of lofted ice contributes to the stratospheric water vapor mixing ratio [Kley et al., 1982; Chaboureau et al., 2007; Corti et al., 2008; Khaykin et al., 2009; Liu et al., 2010b; Schoeberl et al., 2014; Ueyama et al., 2015; Dessler et al., 2016]. Studying the distribution of lofted ice evaporation rate could help us understand where the contributions come from. In this section, we are interested in the lofted ice evaporation rate at 85 hPa (an average of evaporation events between 93 hPa and 79 hPa), a level near the top of the TTL, and at 100 hPa (an average of evaporation events between 93 hPa and 109 hPa), a level near the cold point tropopause (level of minimum temperature), to have a thorough understanding of lofted ice evaporation.

Fig. 3.2 shows that the distribution of the traj_GEOSCCM lofted ice evaporation rate

in the TTL is similar to the lofted ice field in the GEOSCCM (see also fig. 2.2 and 2.3). Overall, the horizontal distribution of the evaporation rate is similar at the 85 hPa and 100 hPa levels, with the evaporation rate decreasing with altitude, as expected. Lofted ice evaporates throughout the tropics, and the highest evaporation rate is located in the monsoon region over Asia during JJA, and over tropical western Pacific and South America during DJF, which are exactly the regions where the lofted ice is abundant. The vertical distribution of lofted ice and the evaporation rate also have some similarities: they are concentrated within the tropics below 60 hPa, and they decrease with latitude and height; the summer hemispheres in both seasons have larger amounts of lofted ice, and a greater evaporation rate (Fig. 3.2 e and f).

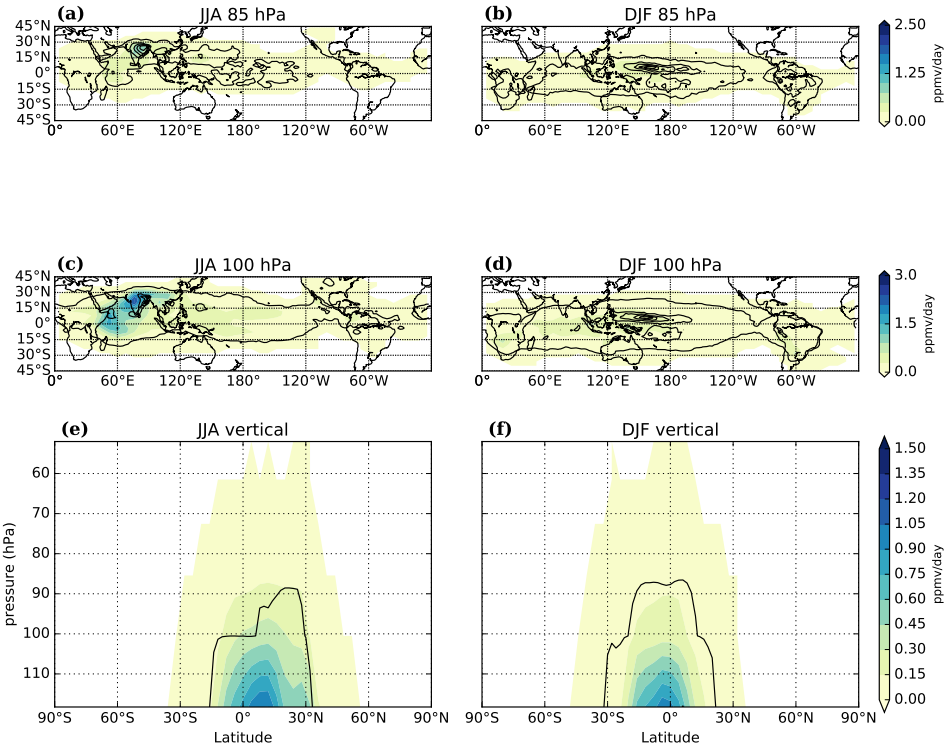

Figure 3.2: Our estimate of lofted ice evaporation rate (ppmv/day) in the traj_GEOSCCM s80 experiment over (a, c and e) 2000-2009 JJA, and (b, d and f) 2000-2009 DJF. (a) and (b) show horizontal distribution at 85 hPa, (c) and (d) show horizontal distribution at 100 hPa, and (e) and (f) show vertical distribution by latitude and pressure. Contours show cloud ice mixing ratio in the GEOSCCM (ppmv).

The rate of evaporation is determined by the amount of ice available to evaporate, but it is also constrained by the convective contrast, which could be revealed by the contrast of lofted ice evaporation rates between different seasons. As we mentioned in chapter 2, the lofted ice mixing ratio is high during DJF (0.007 ppmv, tropical average at 85 hPa) than during JJA (0.005 ppmv, tropical average at 85 hPa), but the convective contrast, especially the convective contrast over the tropical western Pacific (which is the DJF lofted ice center) is extremely low (Fig. 2.5b). As a result, evaporation of convectively lofted ice over this region is limited, and the evaporation rate during DJF (0.058 ppmv/day, tropical average

at 85 hPa) is lower than during JJA (0.069 ppmv/day, tropical average at 85 hPa).

Fig. 3.3 shows that the distribution of the traj_WACCM lofted ice evaporation rate in the TTL is also similar to the lofted ice field in WACCM. The evaporation rate at different levels looks roughly similar, although the magnitude decreases with altitude. We find high evaporation rate areas over the Asian monsoon region during JJA, and over a large area around the tropical western Pacific during DJF. Due to the convective cloud top limit, the lofted ice evaporation rate is zero above 90 hPa. Despite this fact, the vertical distribution of lofted ice mixing ratio and its evaporation rate are also consistent. Also, evaporation over the polar regions is probably not a real addition of water from convection – it results from our classification of all clouds at altitudes below 90 hPa being of convective origin.

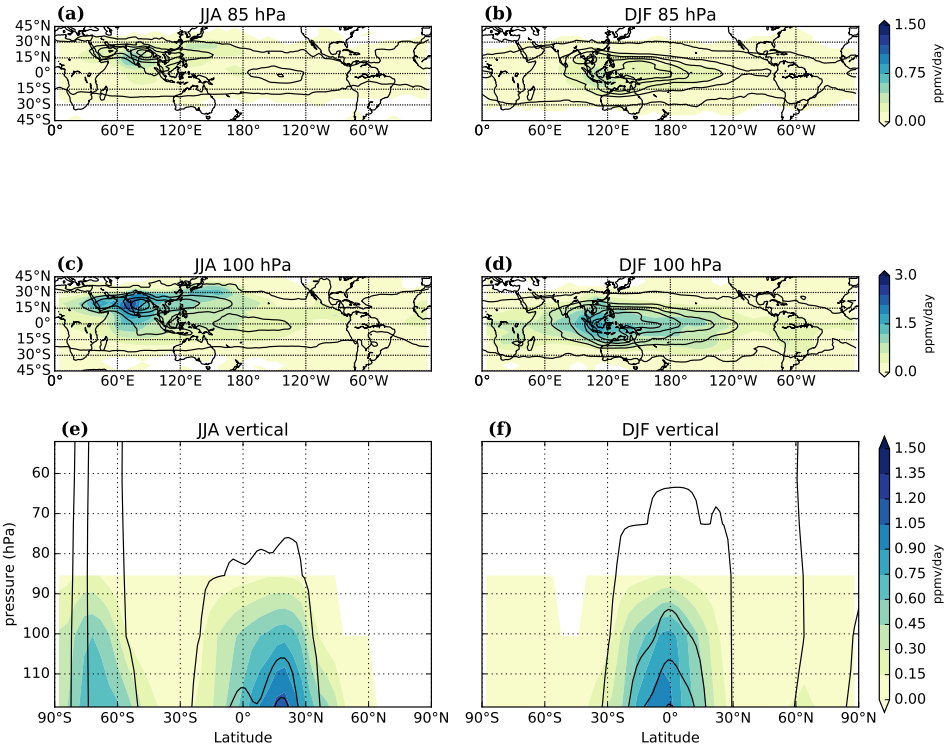

Figure 3.3: Our estimate of lofted ice evaporation rate (ppmv/day) in the traj_WACCM s80 experiments in (a, c and e) JJA 2000-2009, and in (b, d and f) DJF 2000-2009. (a) and (b) show the horizontal distribution at 85 hPa, (c) and (d) show horizontal distribution at 100 hPa, and (e) and (f) show vertical distribution by latitude and pressure. Contours represent cloud ice mixing ratio in WACCM, because of the convective cloud top we set, 90 hPa-cloud is shown in 85 hPa plots.

As with the traj_GEOSCCM, since the lofted ice is mainly over the Asian monsoon regions during JJA, and over the tropical western Pacific during DJF, the convective contrast over these two regions controls the amount of ice evaporation. Although the lofted ice mixing ratio in WACCM during DJF (0.19 ppmv, tropical average at 85 hPa) is much higher than during JJA (0.07 ppmv, tropical average at 85 hPa), the lofted ice evaporation rates are similar during the two seasons (0.078 ppmv/day, tropical average at 85 hPa in DJF, and 0.079 ppmv/day, tropical average at 85 hPa in JJA) because the convective contrast is low during DJF (section 2.4) and this constrains the evaporation of lofted ice.

Furthermore, Our assumptions in section 2.4 is validated, that since the convective contrast over key regions is higher in traj_GEOSCCM, the evaporation rate in traj_GEOSCCM is higher than in traj_WACCM.

To validate the importance of convective contrast to the evaporation rate, we also performed experiments to judge whether the evaporation is 'temperature limited', which means that the value of the evaporation rate is limited by convective contrast, or 'ice limited', which means that the evaporation rate is limited by the amount of lofted ice. We doubled the amount of lofted ice, and we find that in most part of the TTL around the lofted ice centers, the value of evaporation rate of lofted ice changes little with the increase of lofted ice mixing ratio, indicating that the evaporation rate is mainly temperature limited. In the edge of TTL near mid-latitudes, including the northern part of the Asian monsoon regions in the traj_GEOSCCM, the convective contrast is high, and the lofted ice evaporation rate is 'ice limited'.

3.2 Lofted ice net contribution to stratospheric water vapor

As parcels ascend through the TTL, lofted ice can evaporate into the air and increase the water vapor mixing ratio. At the same time, the moister air has a higher chance of saturating and undergoing additional dehydration. So, the rate of evaporation does not tell us how much of that water eventually makes it into the stratosphere. Rather, the net contribution of lofted ice to stratospheric water vapor is also determined by the temperature history of the parcel after its encounter with convection.

We estimate the net contribution of lofted ice as the difference between the H_2O mixing ratio in the run with lofted ice evaporation and the run without. Since parcels enter the stratosphere in the tropics and the evaporation of lofted ice mainly happens in the TTL, we focus first on the net contribution of lofted ice in the tropics. In the traj_GEOSCCM experiments, runs with ice are moister everywhere through the tropics (Fig. 3.4). During

JJA, lofted ice primarily affects water vapor over the Indian Ocean and northern India, regions where both the lofted ice mixing ratio (Fig. 3.4a, contours) and the convective contrast (Fig. 2.5a) are relatively high. During DJF, the center of high net contribution is over Indonesia, a region of both high convective contrast (Fig. 2.5b) and high lofted ice (Fig. 3.4b, contours), and the Indian Ocean, a region of high convective contrast (Fig. 2.5b), but not obvious lofted ice (Fig. 3.4b, contours).

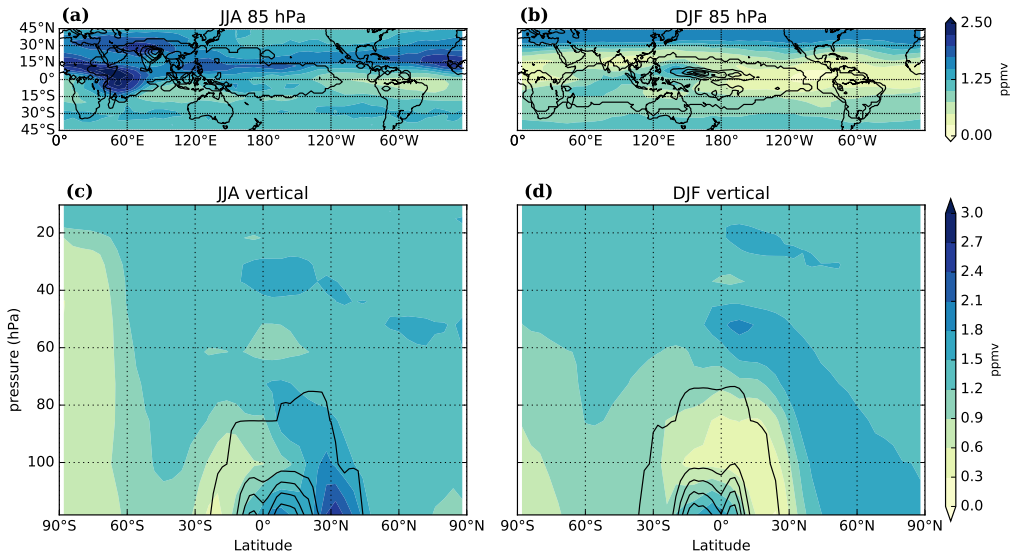

Figure 3.4: The traj_GEOSCCM s80 run result of average net contribution of lofted ice over (a, c) 2000-2009 JJA and (b, d) 2000-2009 DJF. Net contribution of lofted ice is the H_2O mixing ratio difference between the trajectory ice run and the no-ice run. (a) and (b) show horizontal distribution at 85hPa, and (c) and (d) show the vertical distribution by latitude and pressure. Contours show cloud ice mixing ratio in the GEOSCCM.

In traj_WACCM experiments, the runs with ice also moisten everywhere throughout the tropics (Fig. 3.5). During JJA, the net contribution of lofted ice occurs mainly over the Indian Ocean and the northern Pacific, which are the regions of relatively high lofted ice mixing ratio and relatively high convective contrast. During DJF, the net contribution is

also distributed throughout the tropics, except over western Pacific, sharing a distribution similar to the convective contrast (Fig. 2.5) but substantially different from the lofted ice mixing ratio (Figs. 2.2 and 2.3).

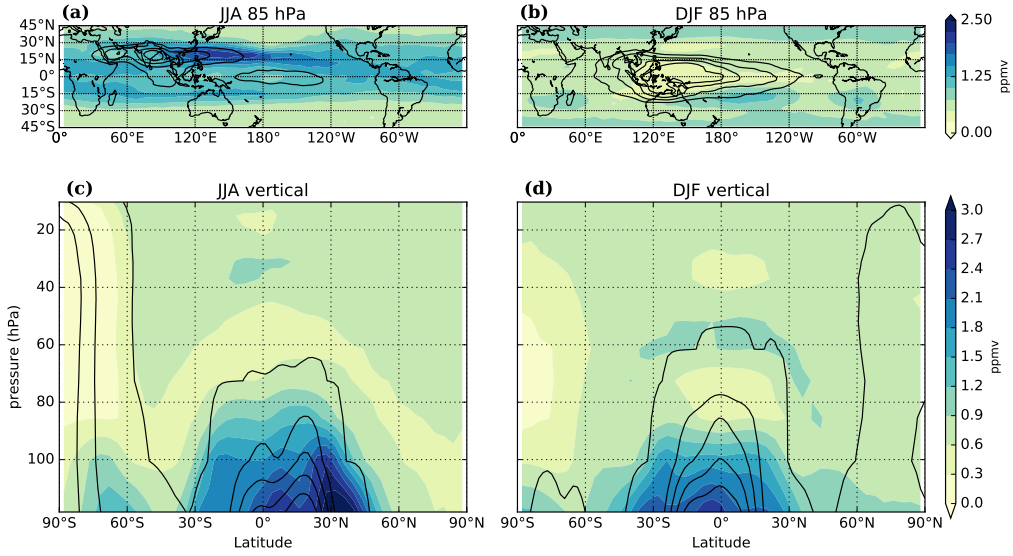

Figure 3.5: The traj_WACCM s100 run result of average net contribution of lofted ice over (a, b) 2000-2009 JJA and (c, d) 2000-2009 DJF. Net contribution of lofted ice is the H_2O mixing ratio difference between the trajectory ice run and the no-ice run. (a) and (b) show horizontal distribution at 85 hPa, and (c) and (d) show the vertical distribution by latitude and pressure. Contours show cloud ice mixing ratio in the WACCM, because of the convective cloud top we set, 90 hPa-cloud is shown in 85 hPa plots.

The horizontal distribution of net contribution looks 'better-mixed' than the evaporation events, and shares more similarities with the distribution of convective contrast rather than lofted ice mixing ratio. The horizontal air motion near the two key regions of lofted ice evaporation is rapid [Fueglistaler et al., 2009], and the large scale anticyclones over the Asian monsoon region and the tropical western Pacific transport air to other part of the TTL [Hatsushika and Yamazaki, 2003; Garny and Randel, 2016]. Parcels moistened by

lofted ice over key regions are advected throughout the TTL.

To have a better understanding of the horizontal transport of the net effect of lofted ice, we performed several regional evaporation tests where evaporation of lofted ice is allowed only in key regions: the Asian monsoon region (referred to as traj_GEOSCCM_AS runs and traj_WACCM_AS runs) or the tropical western Pacific (referred to as traj_GEOSCCM_TWP runs and traj_WACCM_TWP runs). The net contribution of these regional evaporation tests is shown in Fig. 3.6. The evaporated lofted ice over both the Asian monsoon region and the tropical western Pacific can be transported throughout the tropics. During JJA, the evaporated lofted ice increases water vapor in the northern hemisphere. It is then transported eastward through the Middle East and North Africa and reaches the Atlantic Ocean. During DJF, the entire tropics is influenced by lofted ice evaporation above the tropical western Pacific, especially the Indian Ocean. In conclusion, the evaporated lofted ice can contribute to water vapor mixing ratio globally, but most of the contributions are near the evaporation key regions, only small amount of evaporated lofted ice is transported to regions far away.

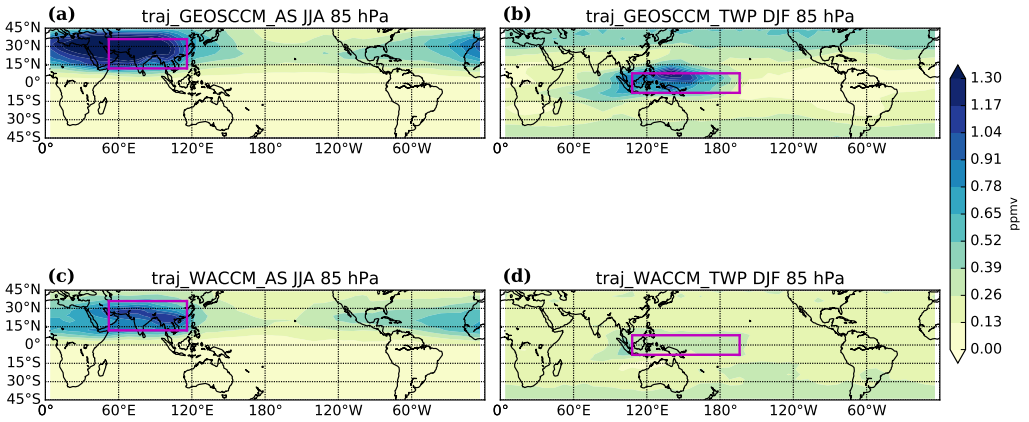

Figure 3.6: The net contribution of lofted ice in four regional evaporation tests at 85 hPa. (a) traj_GEOSCCM_AS s80 run, during JJA; (b) shows in traj_GEOSCCM_TWP s80 run, during DJF; (c) shows in traj_WACCM_AS s100 run, during JJA; (d) shows in traj_WACCM_TWP s100 run, during DJF. Magenta contours indicate the regions where lofted ice is allowed to evaporate in each panel.

Experiments that double the amount of lofted ice prove that the net contribution of lofted ice is also temperature limited in most regions of the TTL in both traj_GEOSCCM and traj_WACCM. Regions with low convective contrast have air that is near saturated, and remote ice evaporation transported to that region can seldom increase water vapor; regions with high convective contrast has less saturated air, and can be moistened by remote evaporated air transported here. The Indian Ocean region during both boreal summer and winter, and the northern Pacific during JJA, are temperature limited regions with both high lofted ice abundance and high convective contrast, so lofted ice can moisten these regions most. In addition, few regions far from the lofted ice centers experience less frequent convection and are ice limited.

Double lofted ice experiments also show that net contribution during DJF is more temperature limited than during JJA, because of the TTL temperature during DJF is lower than

during JJA. Doubling the lofted ice mixing ratio, TTL average net contribution increases by 3.9% (in traj_GEOSCCM) or 1.8% (in traj_WACCM) of its original value during JJA, and increases 2.2% (in traj_GEOSCCM) or 1.2% (in traj_WACCM) of its original value during DJF.

Although convection and cloud ice evaporation mainly occurs in the TTL, their impact can be transported throughout the stratosphere and mid-latitudes by the general circulation (fig. 3.4c and d, fig. 3.5c and d). The net contribution of lofted ice in the TTL is larger during JJA than during DJF, and the seasonal variability of the net contribution on TTL water vapor from lofted ice is imprinted in the stratosphere, like the canonical tape recorder. This is why the vertical distribution of the net contribution of lofted ice shown in fig. 3.4c and d and fig. 3.5c and d shows vertical layering of low and high contribution. As a result of the general circulation, the net contribution of lofted ice in mid-latitudes also shows a layered structure. This layered structure extends through the Arctic during both DJF and JJA. In Antarctica, low temperature cause local dehydration, which is primarily responsible for the structure of the water vapor distribution there.

3.3 Comparison of lofted ice contribution from different layers

To better quantify the altitude where evaporation of lofted ice has the largest contribution, we divide the TTL into four isentropic layers: between 370 K and 380 K, between 380 K and 390 K, between 390 K and 400 K, and above 400 K. As the lowest layer we choose 370 K to 380 K because parcels are initiated at 370 K in our experiments, so our model does not tell us anything about convection at lower altitudes. In addition, it is unlikely that lower altitude convection will have a big impact on stratospheric water vapor [Dessler et al., 2007].

We run four level-dependent evaporation experiments where we only allow lofted ice to evaporate in one of these layers. The runs are named for the layers where ice is allowed

to evaporate; for example, the runs where lofted ice can only evaporate when parcels are between the 370 K and 380 K isentrope are called the evap_370_380 runs.

The tropical average lofted ice mixing ratio in the four layers and the ratio of their mass fraction to total lofted ice in the GEOSCCM is shown in Table 3.2. As shown in figs. 2.2 and 2.3, the amount of cloud ice decreases with potential temperature: $\sim$85% of lofted ice is between 370 K and 380 K, and only a few clouds penetrate above 400 K.

The tropical average lofted ice mixing ratios in the four layers and their proportions to total lofted ice in WACCM are also shown in Table 3.2. Values are only estimates for the WACCM given that we assume any ice at altitudes below 90 hPa originates from convection and any ice above is formed in situ. This is why the amount of lofted ice above 390 K is nearly zero. Because of this, the lofted ice between 370 K and 380 K accounts for $\sim$99% of total lofted ice, with lofted ice between 380 K and 390 K accounting for the rest.

Table 3.2: Tropical average lofted cloud ice mixing ratio and the mass fraction of total lofted ice between 370 K and 400 K in CCMs in that layer averaged over 2000 to 2009: 370 K to 380 K, 380 K to 390 K, 390 K to 400 K, and above 400 K (ppmv). As previously discussed, convective clouds in WACCM are assumed to be zero above 90 hPa.

	GEOSCCM		WACCM	
	mixing ratio (ppmv)	fraction	mixing ratio (ppmv)	fraction
370-380	0.0189	85.57%	0.1974	98.23%
380-390	0.0025	11.34%	0.0036	1.77%
390-400	0.0006	2.53%	<1e-6	$\sim$0
400+	0.0001	0.56%	<1e-14	$\sim$0

Fig. 3.7a shows the tropical average net contribution of lofted ice in the four

traj_GEOSCCM level-dependent evaporation runs and in the ice run where ice in all levels is allowed to evaporate. The spatial patterns of the net contribution in all level-dependent evaporation experiments are similar as shown in section 3.2. In the level-dependent evaporation runs, above the evaporation layer the net contribution decreases with height, because parcels are being exposed to cold temperatures and some are being dehydrated. The annual average of the net contribution above 70 hPa is similar for all layers, because convective cloud can not penetrate into that altitude, and because temperature here is high and the already evaporated lofted ice would not dehydrate away above 70 hPa. As a result, the net contribution on a certain level above 70 hPa can represent the total net contribution to stratospheric water vapor in a certain experiment.

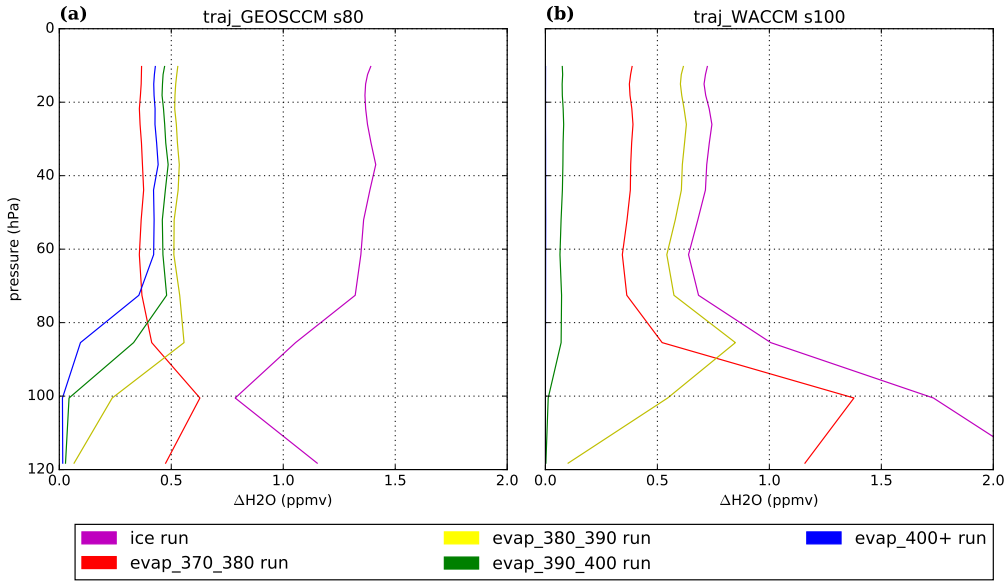

Figure 3.7: Tropical net contribution of lofted ice in four level-dependent evaporation runs and in the ice run from 2000 to 2009. Level-dependent evaporation experiments contain: the evap_370_380 run, the evap_380_390 run, the evap_390_400 run, the evap_400+ run. (a) shows traj_GEOSCCM result, (b) shows traj_WACCM result.

Table 3.3 shows the net contribution of lofted ice on 52-hPa water vapor. Table 3.3 also contains the proportion of net contribution in each level-dependent experiment to total net contribution of four level-dependent evaporation experiments. The sum of lofted ice net contribution of individual layers is 29.74% (in traj_GEOSCCM) or 47.62% larger than in the run that allows lofted ice evaporating in all layers, indicating that same air is less likely rehydrated in the run that allow lofted ice evaporating in all layers.

Table 3.3: Tropical net contribution of lofted ice in several trajectory runs over 2000-2009 at 52 hPa (ppmv) and their proportion to total net contribution. Here total net contribution is the sum of net contribution in four level-dependent evaporation experiments.

	traj_GEOSCCM s80		traj_WACCM s100	
	ΔH_2O (ppmv)	fraction	ΔH_2O (ppmv)	fraction
evap_370_380 run	0.365	20.74%	0.365	35.88%
evap_380_390 run	0.512	29.09%	0.580	57.07%
evap_390_400 run	0.460	26.11%	0.070	6.90%
evap_400+ run	0.423	24.03%	0.002	0.14%
ice run	1.359	77.08%	0.681	67.74%

Adding lofted ice in these four layers moistens the stratosphere by $\sim$0.4–0.5 ppmv. This means that although the amount of lofted ice and the degree of subsaturation differs between the layers, the net contribution from each layer is similar. Evaporated cloud ice from below the cold point tropopause (in the evap_370_380 run), contributes 20.74% of the total net contribution to stratospheric water vapor, which is the least among four level-dependent evaporation experiments, because parcels tend to experience further dehydration and lose water vapor. The tropical average H_2O mixing ratio of the evap_380_390 run

result is highest among these 4 experiments by contributing 29.09% of net contribution, indicating that the layer just above the tropopause, makes the greatest contribution. This is also consistent with the result of Dessler et al. [2007].

Since there is almost no lofted ice above 390 K, the net contributions in traj_WACCM evap_390_400 and evap_400+ experiments are near zero, and do not have a clear distribution pattern. The pattern of the net contribution of lofted ice in other traj_WACCM level-dependent evaporation runs is consistent with the ice run shown in section 3.2. Fig. 3.7b shows that in the TTL, hydration from lofted ice and dehydration when crossing the cold region cause the net contribution of lofted ice in all traj_WACCM experiments to first increase and then decrease with height. The net contribution is consistent in all levels, above 70 hPa in the stratosphere.

In the traj_WACCM, evaporated cloud ice from the 370K to 380K layer has a limited impact on stratospheric water vapor and only moistens the stratosphere by 0.365 ppmv, 35.88% of the total net contribution. The contribution from lofted ice between 380 K and 390 K, is largest in traj_WACCM, 57.07%, because lofted ice evaporating here encounters less subsequent dehydration and therefore makes a larger contribution to stratospheric water vapor. The result of the traj_WACCM runs also shows that, although the amount of lofted ice below the cold point tropopause accounts for a great proportion to total lofted ice, the lofted ice above the cold point tropopause is what acts to moisten the stratosphere.

Generally, although convectively lofted clouds penetrate the tropopause infrequently, the small amount of lofted ice above the cold point tropopause plays a key role in determining the stratospheric H_2O mixing ratio, and the most important layer is the layer right above the cold point tropopause due to its abundant lofted ice. Convectively lofted ice below the tropopause makes a smaller contribution.

3.4 Lofted ice impact on final dehydration location density

Parcels may dehydrate several times as they cross the TTL, but it is the final dehydration event that determines the parcel's final water vapor concentration. We define a dehydration event to be the final dehydration event if no further dehydration happens within the following year (365 days). Schoeberl and Dessler [2011] showed that most of the final dehydration events in a model without convective ice lofting are distributed near the cold point tropopause and mostly occur above the tropical western Pacific and South America.

In this section, the problem we are interested in is how the evaporation of lofted ice influences the final dehydration location density. Fig. 3.8a shows the final dehydration location density horizontal distribution difference between the 2000-2009 traj_GEOSCCM ice run and no-ice run, and fig. 3.8c shows the vertical distribution difference. Adding evaporated lofted ice to the model, the location of final dehydration migrates from the tropical western Pacific, and South America, the cold centers and low convective contrast areas, to the Indian Ocean and East Africa, areas with lofted ice evaporation and with high convective contrast. The final dehydration location density tends to decrease at 100 hPa, and increase at 80 hPa.

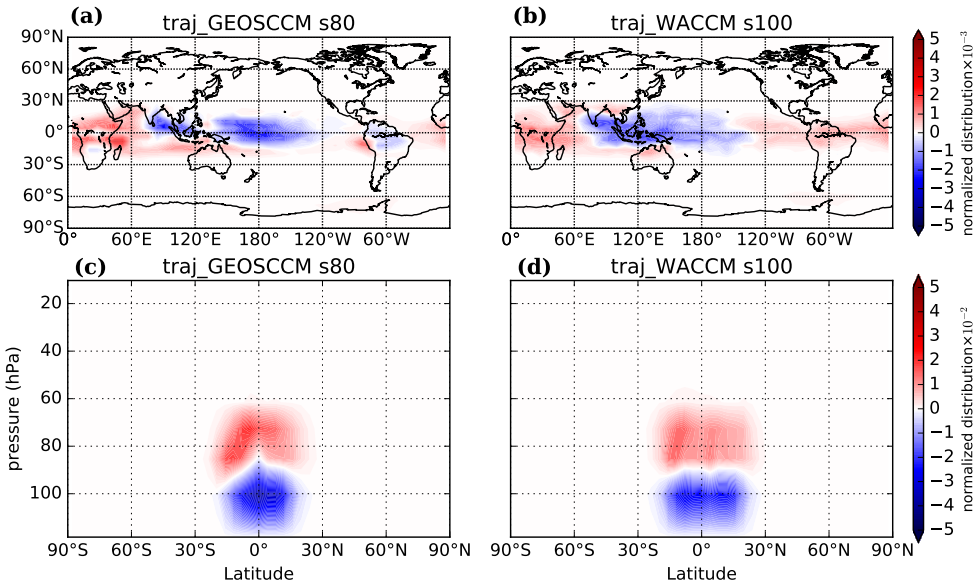

Figure 3.8: Final dehydration location density difference between the trajectory lofted ice runs and no-ice runs in traj_GEOSCCM s80 (a, c) and traj_WACCM s100 (b, d) over 2000-2009. (a, b) shows the horizontal distribution of total final dehydration location density difference, and (c, d) shows the change in the vertical distribution. We calculate the final dehydration location density by binning the final dehydration locations into latitude-longitude and latitude-pressure grids, and normalize every experiment by the total final dehydrated parcel numbers.

Similar conclusions could also be drawn from the traj_WACCM results (fig. 3.8b and d): after adding lofted ice, the location of final dehydration migrates from near the cold point tropopause to above the cold point tropopause, and from low convective contrast areas (tropical western Pacific) to high convective contrast areas (Indian Ocean, East Africa, and South America).

The location of the Lagrangian cold point in parcels' trajectories are the final dehydration locations in the no-ice runs, and parcels will enter the stratosphere carrying the temperature information of the Lagrangian cold point. The migration of the final density locations in ice runs indicates that if the evaporated lofted ice is added after crossing the

Lagrangian cold point, it may encounter further dehydration and carry the temperature information of warmer regions rather than of the Lagrangian cold point, and thus moisten the stratosphere.

4. CHANGES IN LOFTED ICE IMPACT DURING THE 21ST CENTURY

Almost all models predict that H_2O_{entry} will increase through 21st century [Gettelman et al., 2010; Kim et al., 2013], which will tend to increase stratospheric water vapor. An increase in lofted ice evaporation above the cold point tropopause is one of the factors that are responsible for the increase of H_2O_{entry} [Dessler et al., 2016]; the other factor is warming temperatures of the TTL. Using the trajectory model to show where the increase occurs, due to the change of lofted ice evaporation, is another aim of this thesis.

In both GEOSCCM and WACCM, the amount of convectively lofted ice increases over the 21st century. Fig. 4.1a and b show the difference of the lofted ice mixing ratio between 2089-2098 and 2000-2009 at 85 hPa in CCMs (as introduced in section 2, anvil ice in GEOSCCM, lofted ice and ice formed in situ in WACCM). The increase in lofted ice mixing ratio over the 21st century follows the pattern of ice in the first decade, indicating that places with lofted ice get more, while places without it continue to have little. The key regions of high lofted ice concentration are still the Asian monsoon region and tropical western Pacific.

The evaporation rate increases over the 21st century (Fig. 4.1c and d). In Section 3.1, we showed that the distribution of the lofted ice evaporation rate follows the distribution of the lofted ice in CCMs, so it is not surprising that the increase of lofted ice evaporation rate also follows the previous distribution pattern. The Asian monsoon region during JJA, and the tropical western Pacific region during DJF, remain key regions of lofted ice evaporation over the last decade in 21st century, and will contribute more water to the TTL.

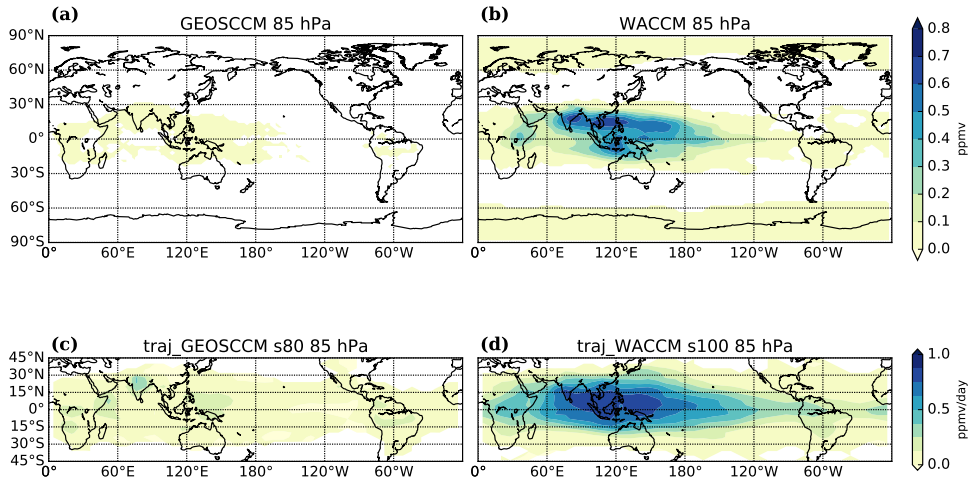

Figure 4.1: (a, b) The difference of average cloud ice mixing ratio between the first decade and last decade of 21st century at 85 hPa in (a) GEOSCCM output and (b) WACCM output. (c, d) The difference of lofted ice evaporation rate in trajectory experiments between 2000-2009 and 2089-2098 at 85 hPa in: (c) traj_GEOSCCM s80 run and (d) traj_WACCM s100 run. 100 hPa plots look the same.

Except for the increase of lofted ice mixing ratio, the increase in convective contrast also explains part of the increase of lofted ice evaporation rate over 21st century, since the amount of evaporation is temperature limited over the lofted ice key regions. Almost all models [Santer et al., 2003; Gettelman et al., 2010], including GEOSCCM and WACCM, show a warmer troposphere, warmer cold point tropopause, and colder stratosphere in the last decade of the 21st century. As is introduced in chapter 2, the convective contrast is the difference between water vapor mixing ratio and the saturated water vapor mixing ratio in a no-ice run. The saturated water vapor mixing ratio is determined by the temperature at a given position, and water vapor mixing ratio is determined by temperature at the Lagrangian cold point. The saturated water vapor mixing ratio increases exponentially with temperature, in other word, the same increase at high temperatures causes larger change of

saturated water vapor mixing ratio than at low temperatures. As a result, warming around the cold point tropopause leads to an increase of both water vapor mixing ratio and saturated water vapor mixing ratio, but the increase of saturated water vapor mixing ratio is larger, thus increasing the convective contrast (Fig. 4.2).

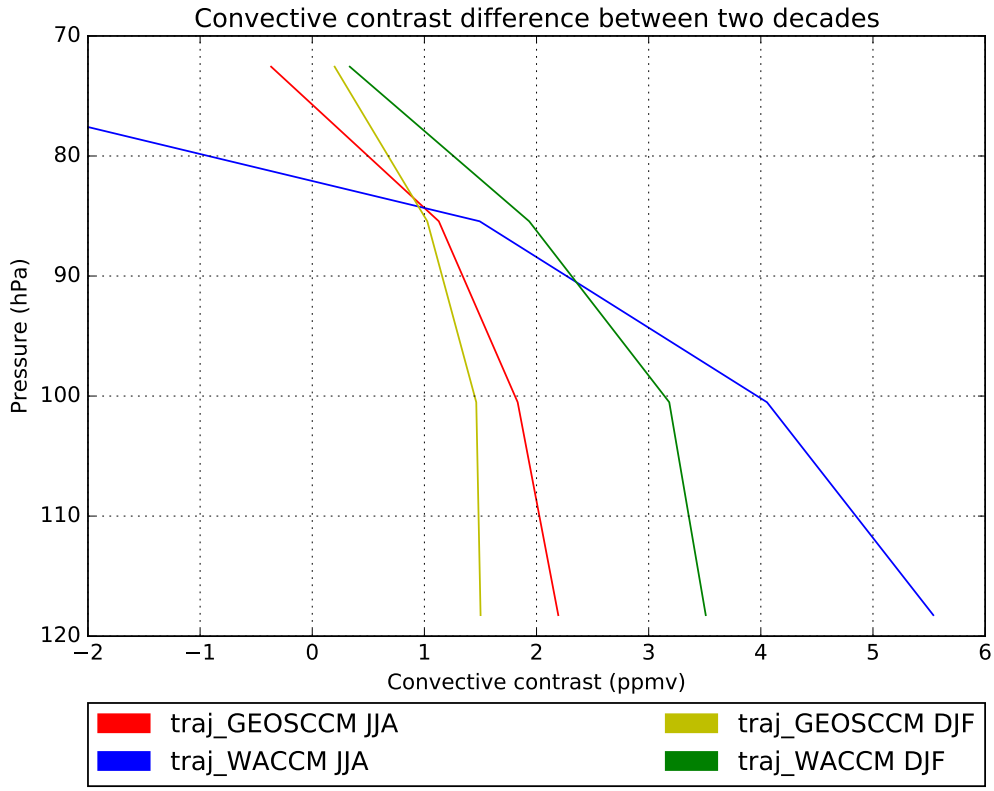

Figure 4.2: The difference of convective contrast in traj_GEOSCCM s80 and traj_WACCM s100, between over 2089-2098 and over 2000-2009.

The increase of the lofted ice mixing ratio and convective contrast over the 21st century below 80 hPa also causes the net contribution in traj_GEOSCCM to increases relatively uniformly over the whole tropics (Fig. 4.3a and b), and the degree of increase is distributed evenly over the previous lofted ice net contribution from 2000-2009. The same conclusion

can also be drawn for the traj_WACCM (Fig. 4.3c and d): the net contribution increases evenly over previous distribution. Because change of convective contrast during DJF in traj_WACCM at 85 hPa is larger than during JJA and in traj_GEOSCCM, net contribution increases greatly during DJF over 21st century in traj_WACCM.

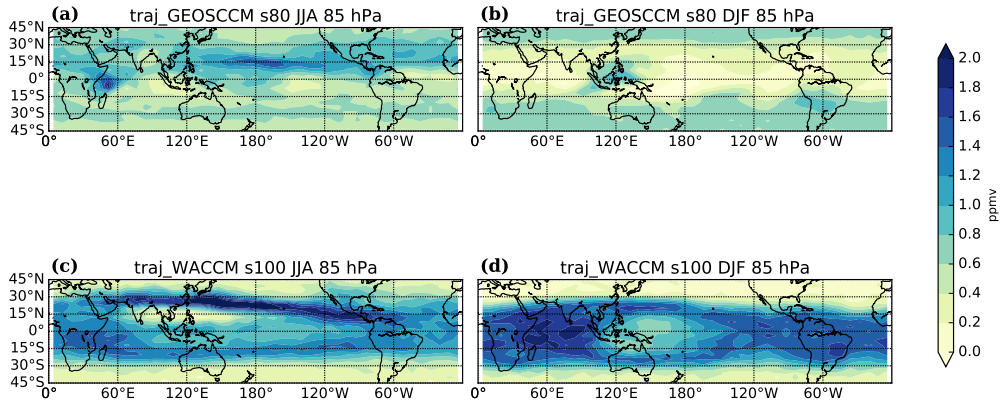

Figure 4.3: The difference of lofted ice net contribution in trajectory experiments between 2000-2009 and 2089-2098 at 85 hPa in: (a, b) traj_GEOSCCM s80, and (c, d) traj_WACCM s100. Left panels show during JJA, and right panels show during DJF. 100 hPa plots look the same.

To conclude, comparing 2089-2098 to 2000-2009, the TTL average temperature increases by about 1K, and the convective contrast increases by 1-2 ppmv correspondingly. On the other hand, lofted ice mixing ratio also increases by 135% (in WACCM) to 140% (in GEOSCCM) of its original value. Since the lofted ice evaporation rate and its net contribution are temperature limited in most regions of the TTL and ice limited in others, the increase of both factors leads to an increase in two variable. The evaporation of lofted ice still occurs over the tropical western Pacific during DJF, and over the Asian monsoon

region during JJA, so the net contribution of evaporation of lofted ice also is largest over the regions around these key regions where the convective contrast is high.

5. CONCLUSIONS

This thesis analyzes the impact of convectively lofted ice on stratospheric water vapor using Lagrangian trajectory model and two chemistry-climate models. Previous work has shown that evaporation of convectively lofted ice plays a key role in the long-term trend of increasing the stratospheric water vapor content in the CCMs [Dessler et al., 2016]. We analyze the location, seasonality, and long-term trends of this evaporation.

The Asian monsoon region and the tropical western Pacific, because of low tropopause temperature, are important regions that control the stratospheric water vapor by controlling dehydration in the TTL [Schoeberl and Dessler, 2011]. In this thesis, we find that they are also key regions where the convectively lofted ice occurs and evaporates in the CCMs. Although the distribution of lofted ice evaporation follows the distribution of lofted ice, its value is temperature limited in these key regions. In other word, the rate of lofted ice evaporation is sensitive to temperature instead of lofted ice mixing ratio.

The net contribution of evaporation of lofted ice is mainly determined by the convective contrast — the capability of being hydrated before adding lofted ice. The areas around the lofted ice key regions with a high convective contrast have larger net contribution. This is then transported throughout the stratosphere by the general circulation.

By dividing the TTL into several layers, we can study the net contribution from each layer individually. We find that the evaporation of lofted ice above the Lagrangian cold point makes the biggest contribution to stratospheric water vapor; the layer just above to the Lagrangian cold point makes the greatest contribution, due to the abundance of lofted ice.

Finally, we explore how lofted ice and its evaporation change over the 21st century. We find that the evaporation rate of lofted ice will have approximately the same geographical

pattern, but will increase in quantity over the 21st century in the CCMs. We also find that the net contribution of lofted ice will increase in quantity, responding to the increase of TTL temperature and convective contrast, contributing to the increase of stratospheric water vapor mixing ratio over the 21st century.

REFERENCES

Alcala, C. M. and Dessler, A. E. (2002). Observations of deep convection in the tropics using the tropical rainfall measuring mission (trmm) precipitation radar. *Journal of Geophysical Research: Atmospheres*, 107(D24):AAC 17–1–AAC 17–7. 4792.

Bates, D. R. and Nicolet, M. (1950). The photochemistry of atmospheric water vapor. *Journal of Geophysical Research*, 55(3):301–327.

Bonazzola, M. and Haynes, P. H. (2004). A trajectory-based study of the tropical tropopause region. *Journal of Geophysical Research: Atmospheres*, 109(D20):n/a–n/a. D20112.

Bowman, K. P. (1993). Large-scale isentropic mixing properties of the antarctic polar vortex from analyzed winds. *Journal of Geophysical Research: Atmospheres*, 98(D12):23013–23027.

Bowman, K. P. and Carrie, G. D. (2002). The mean-meridional transport circulation of the troposphere in an idealized gcm. *Journal of the atmospheric sciences*, 59(9):1502–1514.

Brewer, A. (1949). Evidence for a world circulation provided by the measurements of helium and water vapour distribution in the stratosphere. *Quarterly Journal of the Royal Meteorological Society*, 75(326):351–363.

Chaboureau, J.-P., Cammas, J.-P., Duron, J., Mascart, P. J., Sitnikov, N. M., and Voessing, H.-J. (2007). A numerical study of tropical cross-tropopause transport by convective overshoots. *Atmospheric Chemistry and Physics*, 7(7):1731–1740.

Corti, T., Luo, B. P., de Reus, M., Brunner, D., Cairo, F., Mahoney, M. J., Martucci, G., Matthey, R., Mitev, V., dos Santos, F. H., Schiller, C., Shur, G., Sitnikov, N. M., Spelten, N., Vössing, H. J., Borrmann, S., and Peter, T. (2008). Unprecedented evidence for deep convection hydrating the tropical stratosphere. *Geophysical Research Letters*,

35(10):n/a–n/a. L10810.

Danielsen, E. F. (1982). A dehydration mechanism for the stratosphere. *Geophysical Research Letters*, 9(6):605–608.

de F. Forster, P. M. and Shine, K. P. (1999). Stratospheric water vapour changes as a possible contributor to observed stratospheric cooling. *Geophysical Research Letters*, 26(21):3309–3312.

Dessler, A., Schoeberl, M., Wang, T., Davis, S., and Rosenlof, K. (2013). Stratospheric water vapor feedback. *Proceedings of the National Academy of Sciences*, 110(45):18087–18091.

Dessler, A., Ye, H., Wang, T., Schoeberl, M., Oman, L., Douglass, A., Butler, A., Rosenlof, K., Davis, S., and Portmann, R. (2016). Transport of ice into the stratosphere and the humidification of the stratosphere over the 21st century. *Geophysical Research Letters*, 43(5):2323–2329. 2016GL067991.

Dessler, A. E. (2002). The effect of deep, tropical convection on the tropical tropopause layer. *Journal of Geophysical Research: Atmospheres*, 107(D3):ACH 6–1–ACH 6–5.

Dessler, A. E., Hanisco, T. F., and Fueglistaler, S. (2007). Effects of convective ice lofting on h2o and hdo in the tropical tropopause layer. *Journal of Geophysical Research: Atmospheres*, 112(D18):n/a–n/a. D18309.

Dessler, A. E., Schoeberl, M. R., Wang, T., Davis, S. M., Rosenlof, K. H., and Vernier, J.-P. (2014). Variations of stratospheric water vapor over the past three decades. *Journal of Geophysical Research: Atmospheres*, 119(22):12,588–12,598. 2014JD021712.

Dessler, A. E. and Sherwood, S. C. (2004). Effect of convection on the summertime extratropical lower stratosphere. *Journal of Geophysical Research: Atmospheres*, 109(D23):n/a–n/a. D23301.

Dessler, A. E., Weinstock, E. M., Hintsa, E. J., Anderson, J. G., Webster, C. R., May, R. D., Elkins, J. W., and Dutton, G. S. (1994). An examination of the total hydrogen

budget of the lower stratosphere. *Geophysical Research Letters*, 21(23):2563–2566.

Dvortsov, V. L. and Solomon, S. (2001). Response of the stratospheric temperatures and ozone to past and future increases in stratospheric humidity. *Journal of Geophysical Research: Atmospheres*, 106(D7):7505–7514.

Evans, S. J., Toumi, R., Harries, J. E., Chipperfield, M. R., and Russell, J. M. (1998). Trends in stratospheric humidity and the sensitivity of ozone to these trends. *Journal of Geophysical Research: Atmospheres*, 103(D8):8715–8725.

Fleming, E. L., Jackman, C. H., Weisenstein, D. K., and Ko, M. K. W. (2007). The impact of interannual variability on multidecadal total ozone simulations. *Journal of Geophysical Research: Atmospheres*, 112(D10):n/a–n/a. D10310.

Forster, P. M. d. F. and Shine, K. P. (2002). Assessing the climate impact of trends in stratospheric water vapor. *Geophysical Research Letters*, 29(6):10–1–10–4.

Fueglistaler, S., Dessler, A. E., Dunkerton, T. J., Folkins, I., Fu, Q., and Mote, P. W. (2009). Tropical tropopause layer. *Reviews of Geophysics*, 47(1):n/a–n/a. RG1004.

Fueglistaler, S. and Haynes, P. H. (2005). Control of interannual and longer-term variability of stratospheric water vapor. *Journal of Geophysical Research: Atmospheres*, 110(D24):n/a–n/a. D24108.

Garny, H. and Randel, W. J. (2016). Transport pathways from the asian monsoon anticyclone to the stratosphere. *Atmospheric Chemistry and Physics*, 16(4):2703–2718.

Geller, M. A., Zhou, X., and Zhang, M. (2002). Simulations of the interannual variability of stratospheric water vapor. *Journal of the Atmospheric Sciences*, 59(6):1076–1085.

Gettelman, A., Hegglin, M. I., Son, S.-W., Kim, J., Fujiwara, M., Birner, T., Kremser, S., Rex, M., Añel, J., Akiyoshi, H., et al. (2010). Multimodel assessment of the upper troposphere and lower stratosphere: Tropics and global trends. *Journal of Geophysical Research: Atmospheres*, 115(D3):n/a–n/a.

Gettelman, A., Salby, M. L., and Sassi, F. (2002). Distribution and influence of convec-

tion in the tropical tropopause region. *Journal of Geophysical Research: Atmospheres*, 107(D10):ACL 6–1–ACL 6–12.

Grosvenor, D., Choularton, T., Coe, H., and Held, G. (2007). A study of the effect of overshooting deep convection on the water content of the ttl and lower stratosphere from cloud resolving model simulations. *Atmospheric Chemistry and Physics*, 7(18):4977–5002.

Gunson, M., Farmer, C. B., Norton, R., Zander, R., Rinsland, C. P., Shaw, J., and Gao, B.-C. (1990). Measurements of ch4, n2o, co, h2o, and o3 in the middle atmosphere by the atmospheric trace molecule spectroscopy experiment on spacelab 3. *Journal of Geophysical Research: Atmospheres*, 95(D9):13867–13882.

Hansen, A. R. and Robinson, G. (1989). Water vapor and methane in the upper stratosphere: An examination of some of the nimbus 7 measurements. *Journal of Geophysical Research: Atmospheres*, 94(D6):8474–8484.

Hatsushika, H. and Yamazaki, K. (2003). Stratospheric drain over indonesia and dehydration within the tropical tropopause layer diagnosed by air parcel trajectories. *Journal of Geophysical Research: Atmospheres*, 108(D19):n/a–n/a. 4610.

Hurrell, J. W., Holland, M. M., Gent, P. R., Ghan, S., Kay, J. E., Kushner, P., Lamarque, J.-F., Large, W. G., Lawrence, D., Lindsay, K., et al. (2013). The community earth system model: a framework for collaborative research. *Bulletin of the American Meteorological Society*, 94(9):1339–1360.

Jones, R., Pyle, J., Harries, J., Zavody, A., Russell, J., and Gille, J. (1986). The water vapour budget of the stratosphere studied using lims and sams satellite data. *Quarterly Journal of the Royal Meteorological Society*, 112(474):1127–1143.

Keith, D. W. (2000). Stratosphere-troposphere exchange: Inferences from the isotopic composition of water vapor. *Journal of Geophysical Research: Atmospheres*, 105(D12):15167–15173.

Khaykin, S., Pommereau, J.-P., Korshunov, L., Yushkov, V., Nielsen, J., Larsen, N., Christensen, T., Garnier, A., Lukyanov, A., and Williams, E. (2009). Hydration of the lower stratosphere by ice crystal geysers over land convective systems. *Atmospheric Chemistry and Physics*, 9(6):2275–2287. doi: 10.5194/acp-9-2275-2009.

Kim, J., Grise, K. M., and Son, S.-W. (2013). Thermal characteristics of the cold-point tropopause region in cmip5 models. *Journal of Geophysical Research: Atmospheres*, 118(16):8827–8841.

Kley, D., Schmeltekopf, A. L., Kelly, K., Winkler, R. H., Thompson, T. L., and McFarland, M. (1982). Transport of water through the tropical tropopause. *Geophysical Research Letters*, 9(6):617–620.

Le Texier, H., Solomon, S., and Garcia, R. (1988). The role of molecular hydrogen and methane oxidation in the water vapour budget of the stratosphere. *Quarterly Journal of the Royal Meteorological Society*, 114(480):281–295.

Liu, C. and Zipser, E. J. (2005). Global distribution of convection penetrating the tropical tropopause. *Journal of Geophysical Research: Atmospheres*, 110(D23):n/a–n/a. D23104.

Liu, N. and Liu, C. (2016). Global distribution of deep convection reaching tropopause in 1 year gpm observations. *Journal of Geophysical Research: Atmospheres*, 121(8):3824–3842. 2015JD024430.

Liu, X. M., Rivière, E. D., Marécal, V., Durry, G., Hamdouni, A., Arteta, J., and Khaykin, S. (2010a). Stratospheric water vapour budget and convection overshooting the tropopause: modelling study from scout-amma. *Atmospheric Chemistry and Physics*, 10(17):8267–8286.

Liu, X. M., Rivière, E. D., Marécal, V., Durry, G., Hamdouni, A., Arteta, J., and Khaykin, S. (2010b). Stratospheric water vapour budget and convection overshooting the tropopause: modelling study from scout-amma. *Atmospheric Chemistry and*

Physics, 10(17):8267–8286.

Marsh, D. R., Mills, M. J., Kinnison, D. E., Lamarque, J.-F., Calvo, N., and Polvani, L. M. (2013). Climate change from 1850 to 2005 simulated in cesm1 (waccm). *Journal of climate*, 26(19):7372–7391.

Maycock, A. C., Joshi, M. M., Shine, K. P., and Scaife, A. A. (2013). The circulation response to idealized changes in stratospheric water vapor. *Journal of Climate*, 26(2):545–561.

Molod, A. (2012). Constraints on the profiles of total water pdf in agcms from airs and a high-resolution model. *Journal of Climate*, 25(23):8341–8352.

Molod, A., Takacs, L., Suarez, M., Bacmeister, J., Song, I.-S., and Eichmann, A. (2012). The geos-5 atmospheric general circulation model: Mean climate and development from merra to fortuna. Technical Report 104606, NASA/TM.

Mote, P. W., Rosenlof, K. H., McIntyre, M. E., Carr, E. S., Gille, J. C., Holton, J. R., Kinnersley, J. S., Pumphrey, H. C., Russell, J. M., and Waters, J. W. (1996). An atmospheric tape recorder: The imprint of tropical tropopause temperatures on stratospheric water vapor. *Journal of Geophysical Research: Atmospheres*, 101(D2):3989–4006.

Moyer, E. J., Irion, F. W., Yung, Y. L., and Gunson, M. R. (1996). Atmos stratospheric deuterated water and implications for troposphere-stratosphere transport. *Geophysical Research Letters*, 23(17):2385–2388.

Neale, R. B., Richter, J. H., Conley, A. J., Park, S., Lauritzen, P. H., Gettelman, A., Williamson, D. L., Vavrus, S. J., Taylor, M. A., Collins, W. D., et al. (2010). Description of the ncar community atmosphere model (cam 4.0). *NCAR Tech. Note,NCAR/TN-485+STR,120pp*.

Nielsen, J. K., Larsen, N., Cairo, F., Di Donfrancesco, G., Rosen, J. M., Durry, G., Held, G., and Pommereau, J. P. (2007). Solid particles in the tropical lowest stratosphere. *Atmospheric Chemistry and Physics*, 7(3):685–695.

Ramaswamy, V., Schwarzkopf, M., Randel, W., et al. (1996). Fingerprint of ozone depletion in the spatial and temporal pattern of recent lower-stratospheric cooling. *Nature*, 382(6592):616–618.

Randel, W. J., Wu, F., Oltmans, S. J., Rosenlof, K., and Nedoluha, G. E. (2004). Interannual changes of stratospheric water vapor and correlations with tropical tropopause temperatures. *Journal of the Atmospheric Sciences*, 61(17):2133–2148.

Rienecker, M., Suarez, M., Todling, R., Bacmeister, J., Takacs, L., Liu, H.-C., Gu, W., Sienkiewicz, M., Koster, R., Gelaro, R., et al. (2008). The geos-5 data assimilation system documentation of versions 5.0. 1, 5.1. 0, and 5.2. 0. Technical Report 104606, NASA/TM.

Rossow, W. B. and Pearl, C. (2007). 22-year survey of tropical convection penetrating into the lower stratosphere. *Geophysical Research Letters*, 34(4):n/a–n/a. L04803.

Santer, B. D., Sausen, R., Wigley, T. M. L., Boyle, J. S., AchutaRao, K., Doutriaux, C., Hansen, J. E., Meehl, G. A., Roeckner, E., Ruedy, R., Schmidt, G., and Taylor, K. E. (2003). Behavior of tropopause height and atmospheric temperature in models, reanalyses, and observations: Decadal changes. *Journal of Geophysical Research: Atmospheres*, 108(D1):ACL 1–1–ACL 1–22. 4002.

Scaife, A. A., Butchart, N., Jackson, D. R., and Swinbank, R. (2003). Can changes in enso activity help to explain increasing stratospheric water vapor? *Geophysical Research Letters*, 30(17):n/a–n/a. 1880.

Schoeberl, M. and Dessler, A. (2011). Dehydration of the stratosphere. *Atmospheric Chemistry and Physics*, 11(16):8433–8446.

Schoeberl, M. R., Dessler, A. E., and Wang, T. (2012). Simulation of stratospheric water vapor and trends using three reanalyses. *Atmospheric Chemistry and Physics*, 12(14):6475–6487.

Schoeberl, M. R., Dessler, A. E., and Wang, T. (2013). Modeling upper tropospheric

and lower stratospheric water vapor anomalies. *Atmospheric Chemistry and Physics*, 13(15):7783–7793.

Schoeberl, M. R., Dessler, A. E., Wang, T., Avery, M. A., and Jensen, E. J. (2014). Cloud formation, convection, and stratospheric dehydration. *Earth and Space Science*, 1(1):1–17.

Sherwood, S. C. and Dessler, A. E. (2000). On the control of stratospheric humidity. *Geophysical research letters*, 27(16):2513–2516.

Shindell, D. T. (2001). Climate and ozone response to increased stratospheric water vapor. *Geophysical Research Letters*, 28(8):1551–1554.

Smith, C. A., Haigh, J. D., and Toumi, R. (2001). Radiative forcing due to trends in stratospheric water vapour. *Geophysical Research Letters*, 28(1):179–182.

Smith, K., Neely, R., Marsh, D., and Polvani, L. (2014). The specified chemistry whole atmosphere community climate model (sc-waccm). *Journal of Advances in Modeling Earth Systems*, 6(3):883–901.

Solomon, S., Rosenlof, K. H., Portmann, R. W., Daniel, J. S., Davis, S. M., Sanford, T. J., and Plattner, G.-K. (2010). Contributions of stratospheric water vapor to decadal changes in the rate of global warming. *Science*, 327(5970):1219–1223.

Stenke, A. and Grewe, V. (2005). Simulation of stratospheric water vapor trends: impact on stratospheric ozone chemistry. *Atmospheric Chemistry and Physics*, 5(5):1257–1272.

Tao, M., Konopka, P., Ploeger, F., Riese, M., M˝ uller, R., and Volk, C. M. (2015). Impact of stratospheric major warmings and the quasi-biennial oscillation on the variability of stratospheric water vapor. *Geophysical Research Letters*, 42(11):4599–4607. 2015GL064443.

Ueyama, R., Jensen, E. J., Pfister, L., and Kim, J.-E. (2015). Dynamical, convective, and microphysical control on wintertime distributions of water vapor and clouds in the

tropical tropopause layer. *Journal of Geophysical Research: Atmospheres*, 120(19):n/a–n/a.

Van Vuuren, D. P., Edmonds, J., Kainuma, M., Riahi, K., Thomson, A., Hibbard, K., Hurtt, G. C., Kram, T., Krey, V., Lamarque, J.-F., et al. (2011). The representative concentration pathways: an overview. *Climatic change*, 109:5–31.

World Meteorological Organization (2011). scientific assessment of ozone depletion: 2010. Technical Report 52, Geneva, Switzerland.